groups of Arg^{324}, respectively (Figs. 3 and 4). Arg^{324} extends from the N-digit and is buttressed as the surrogate templating residue by a network of hydrogen bonds with Asp^{399} and the 5′ phosphate of the ejected template G. The pattern of hydrogen bonding between dCTP and Arg^{324} is again such that substitution by any other incoming nucleotide would lead to loss of hydrogen bonds, as well as unfavorable electrostatic and steric intrusion. If dCTP were to be replaced by 2′-deoxythymidine 5′-triphosphate (dTTP), it would position two hydrogen bond donors opposite each other [N3-H(T)-H-Nη2(Arg^{324})], whereas substitution by dGTP or dATP would be even more severe, with the larger purine colliding with the guanidinium group of Arg^{324}. By pairing dCTP with an arginine, Rev1 maintains specificity for dCTP over other incoming nucleotides, even opposite an abasic site.

The structure suggests a specific mechanism for Rev1's ability to promote replication through N^2-adducted guanines that obstruct replication. The N^2 group of G can conjugate with a variety of endogenously formed adducts. Indeed, Rev1 has recently been shown to promote replication through an N^2-adducted G, derived from acrolein. Acrolein, an α,β-unsaturated aldehyde, is generated in vivo as the end product of lipid peroxidation and during oxidation of polyamines. The reaction of acrolein with the N^2 of G in DNA followed by ring closure at N1 leads to the formation of the cyclic adduct γ-HOPdG (fig. S2), which presents a strong block to synthesis by DNA polymerases. Rev1, however, incorporates a C opposite this lesion as efficiently as opposite an undamaged G (*12*). The exclusion of template G from the DNA helix places the N^2 of G in a large (solvent-filled) void between the PAD and the fingers domain (Fig. 3), where an adduct such as γ-HOPdG would be sterically unhindered (fig. S2). Indeed, one major role of Rev1 DNA synthetic activity based on an extrahelical G would be to promote replication through a variety of N^2-guanine adducts that sterically impinge on the minor groove. The incorporation of a correct nucleotide opposite an N^2-adducted guanine is ensured by the pairing of dCTP with an arginine. The structure also correlates well with the inhibitory effect that lesions such as O^6-methylguanine and 8-oxoguanine have on Rev1's ability to incorporate C (*2*). Unlike the N^2 group, the O^6 and C8 atoms are relatively buried when template G is evicted from the DNA helix, and almost any adduct at these positions will invariably clash with Rev1.

In the transfer RNA (tRNA) CCA-adding enzyme, both the tRNA backbone and the protein contribute to the specificity of the incoming nucleotide (*24*). The Rev1 structure presents a mechanism for DNA polymerization in which specificity for both the templating and the incoming nucleotide is provided by the protein rather than the DNA. Eukaryotic translesion synthesis polymerases thus use a variety of means of DNA polymerization, which include Watson-Crick base-pairing by Pols η (*25*) and κ (*26*), Hoogsteen base-pairing by Polι (*18, 22*), and protein template–directed synthesis by Rev1 (Fig. 4).

References and Notes

1. J. R. Nelson, C. W. Lawrence, D. C. Hinkle, *Nature* **382**, 729 (1996).
2. L. Haracska, S. Prakash, L. Prakash, *J. Biol. Chem.* **277**, 15546 (2002).
3. S. Prakash, R. E. Johnson, L. Prakash, *Annu. Rev. Biochem.* **74**, 317 (2005).
4. M. T. Washington, R. E. Johnson, S. Prakash, L. Prakash, *J. Biol. Chem.* **274**, 36835 (1999).
5. R. E. Johnson, M. T. Washington, S. Prakash, L. Prakash, *J. Biol. Chem.* **275**, 7447 (2000).
6. R. E. Johnson, S. Prakash, L. Prakash, *Proc. Natl. Acad. Sci. U.S.A.* **97**, 3838 (2000).
7. R. E. Johnson, M. T. Washington, L. Haracska, S. Prakash, L. Prakash, *Nature* **406**, 1015 (2000).
8. A. Tissier *et al.*, *EMBO J.* **19**, 5259 (2000).
9. Y. Zhang, F. Yuan, X. Wu, Z. Wang, *Mol. Cell. Biol.* **20**, 7099 (2000).
10. L. Haracska *et al.*, *Proc. Natl. Acad. Sci. U.S.A.* **98**, 14256 (2001).
11. M. T. Washington, R. E. Johnson, L. Prakash, S. Prakash, *Mol. Cell. Biol.* **24**, 936 (2004).
12. M. T. Washington *et al.*, *Mol. Cell. Biol.* **24**, 6900 (2004).
13. J. Trincao *et al.*, *Mol. Cell* **8**, 417 (2001).
14. B. L. Zhou, J. D. Pata, T. A. Steitz, *Mol. Cell* **8**, 427 (2001).
15. L. F. Silvian, E. A. Toth, P. Pham, M. F. Goodman, T. Ellenberger, *Nat. Struct. Biol.* **8**, 984 (2001).
16. H. Ling, F. Boudsocq, R. Woodgate, W. Yang, *Cell* **107**, 91 (2001).
17. S. N. Uljon *et al.*, *Structure (Cambridge)* **12**, 1395 (2004).
18. D. T. Nair, R. E. Johnson, S. Prakash, L. Prakash, A. K. Aggarwal, *Nature* **430**, 377 (2004).
19. S. Doublie, S. Tabor, A. M. Long, C. C. Richardson, T. Ellenberger, *Nature* **391**, 251 (1998).
20. Y. Li, S. Korolev, G. Waksman, *EMBO J.* **17**, 7514 (1998).
21. T. A. Steitz, *J. Biol. Chem.* **274**, 17395 (1999).
22. D. T. Nair, R. E. Johnson, L. Prakash, S. Prakash, A. K. Aggarwal, *Structure (Cambridge)*, in press.
23. R. J. Roberts, X. Cheng, *Annu. Rev. Biochem.* **67**, 181 (1998).
24. Y. Xiong, T. A. Steitz, *Nature* **430**, 640 (2004).
25. M. T. Washington, S. A. Helquist, E. T. Kool, L. Prakash, S. Prakash, *Mol. Cell. Biol.* **23**, 5107 (2003).
26. W. T. Wolfle *et al.*, *Mol. Cell. Biol.* **25**, 7137 (2005).
27. Single-letter abbreviations for the amino acid residues here are as follows: D, Asp; E, Glu; F, Phe; G, Gly; K, Lys; L, Leu; M, Met; R, Arg; S, Ser; W, Trp; and Y, Tyr.
28. We thank the staff at Brookhaven National Laboratory (beamline X6A) and Advanced Photon Source (beamline 17ID) for facilitating X-ray data collection. We thank C. Escalante, V. Fedorov, S. Lone, and L. Shen for general assistance. This work was supported by grants from the NIH (A.K.A, S.P, and L.P.). The structure has been deposited in the Protein Data Bank with the accession number 2AQ4.

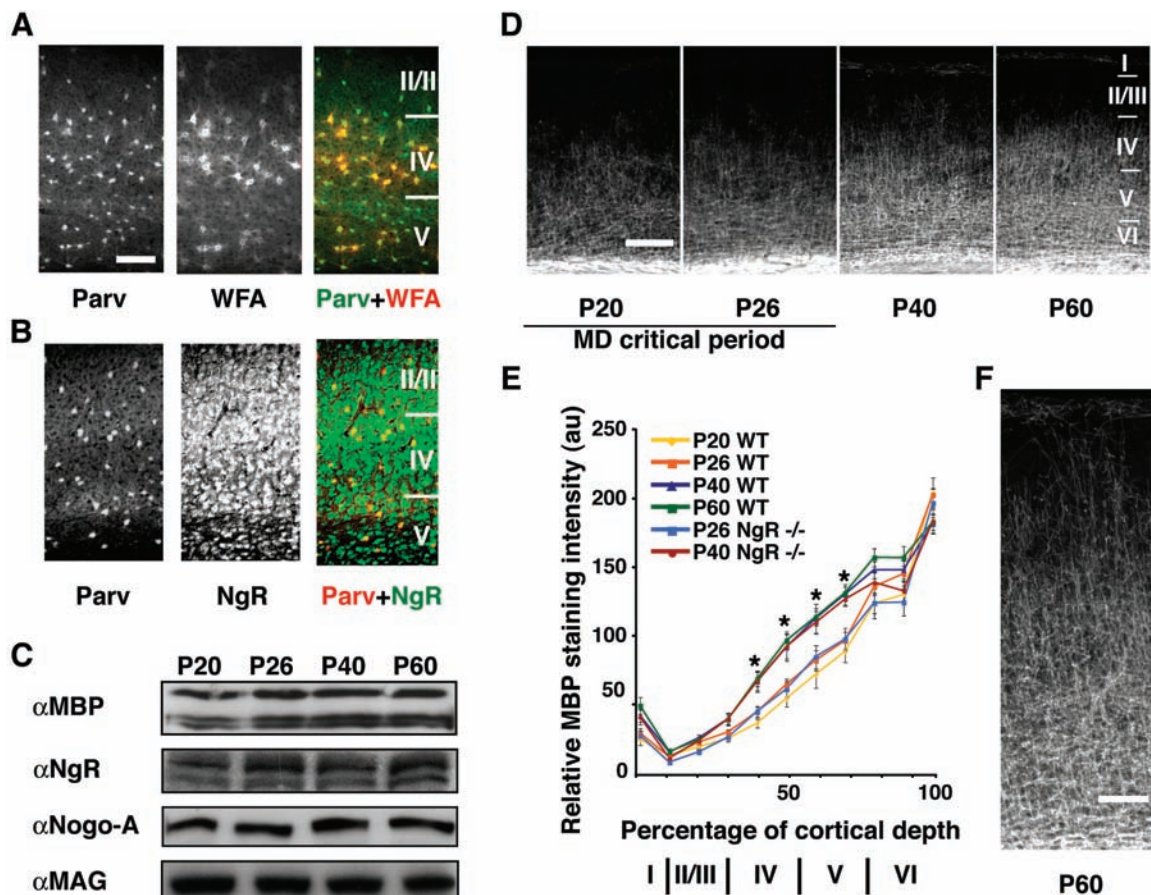# Experience-Driven Plasticity of Visual Cortex Limited by Myelin and Nogo Receptor

Aaron W. McGee,[1]* Yupeng Yang,[2]*† Quentin S. Fischer,[2]‡ Nigel W. Daw,[2] Stephen M. Strittmatter[1]§

Monocular deprivation normally alters ocular dominance in the visual cortex only during a postnatal critical period (20 to 32 days postnatal in mice). We find that mutations in the Nogo-66 receptor (NgR) affect cessation of ocular dominance plasticity. In NgR$^{-/-}$ mice, plasticity during the critical period is normal, but it continues abnormally such that ocular dominance at 45 or 120 days postnatal is subject to the same plasticity as at juvenile ages. Thus, physiological NgR signaling from myelin-derived Nogo, MAG, and OMgp consolidates the neural circuitry established during experience-dependent plasticity. After pathological trauma, similar NgR signaling limits functional recovery and axonal regeneration.

Central nervous system myelin proteins limit axonal growth and regeneration after traumatic and ischemic injury in adult mammals (*1–14*), but a physiological role for the myelin inhibitor pathway has not been defined. Ocular dominance (OD) within visual cortex provides a paradigm to study experience-dependent plasticity. Monocular deprivation of the contralateral eye induces a relative shift in ocular dominance of cortical responses toward the nondeprived ipsilateral eye (*15*). Both anatomical and electrophysiological studies in cats have defined a critical period during which the cerebral cortex is sensitive to experience-dependent plasticity, but after which altered visual experience does not change visual cortex responsiveness (*15–17*). In mice, single-unit recordings under barbiturate anesthesia have revealed a similar critical period for OD between 19 and 32 days postnatal (P19 to P32) (*18–20*). Although mouse OD plasticity measured with this method ceases after P32, a level of adult OD plasticity can be detected by other methods, such as immediate early gene expression and visually evoked potential field

Fig. 1. Expression of myelin, NgR, and CSPG in mouse visual cortex during the critical period for OD plasticity. (**A**) P40 visual cortex labeled for parvalbumin (green in merge) and wisteria floribunda agglutinin (red in merge). (**B**) Sections as in (A), labeled for parvalbumin (red in merge) and NgR (green in merge). (**C**) Homogenates of visual cortex were immunoblotted with the indicated antibodies. Microdensitometry revealed that the concentration of any one protein varied by <20% across these ages, and there were no significant changes in protein levels with age. (**D**) P20 to P60 visual cortex labeled with antibodies to MBP. Layers I to VI are indicated (right). (**E**) Distribution of relative MBP intensity within visual cortex. (**F**) A higher magnification image of MBP distribution at P60.

Error bars reflect SEM; $n = 3$ mice. Asterisks denote significant differences ($P < 0.05$) between P20 and P26 versus P40 and P60 for both genotypes. Scale bars in [(A) and (B)] = 100 μm, in (D) = 200 μm, and in (F) = 100 μm.

recordings (19, 21–23). Adult plasticity is distinct from adolescent critical period plasticity. Adult plasticity relies on the slow onset of strengthened inputs from the nondeprived eye rather than a suppression of responses from the contralateral eye (23). Barbiturate anesthesia masks OD plasticity in adult but not juvenile mice (22). Plasticity achieved during the critical period is more persistent than that obtained in the adult (22). Here, we focus on the abrupt loss of OD plasticity at the end of the critical period in single-unit cortical recordings from anesthetized mice.

Previous investigations have revealed a critical role for parvalbumin-positive γ-aminobutyric acid (GABA)–ergic neurons in timing the critical period. Dark rearing impairs inhibitory circuit maturation (24) and delays the closure of the critical period (25). Genetic disruption of a GABA synthetic enzyme, glutamic acid decarboxylase 65 (GAD65), precludes OD plasticity (26). Brain-derived neurotrophic factor is thought to expedite critical period closure by maturing GABAergic neurons (27). Loss of dendritic spines correlates with OD plasticity and requires both GAD65 function and tissue plasminogen activator (tPA) (28).

Chondroitin sulfate proteoglycans (CSPGs) are astrocyte- and neuron-derived axon-outgrowth inhibitors that have also been implicated in OD plasticity. Infusion of chondroitinase ABC into spinal cord–injured animals cleaves glycosaminoglycan chains and promotes a degree of regeneration and functional recovery (29) comparable to that of Nogo/NgR antagonism (8, 11). Injecting chondroitinase into adult rat visual cortex partially reactivates OD plasticity in response to monocular deprivation (30). To consider the cellular site of CSPG action, we examined wisteria floribunda agglutinin–stained sections of visual cortex. It is remarkable that CSPG-positive perineuronal nets predominantly (>85%) surround parvalbumin-positive inhibitory neurons, leaving nearly all other neurons unencumbered (Fig. 1A). Although genetic and pharmacological manipulation of cortical inhibition supports a model in which parvalbumin-positive inhibitory neurons initiate the critical period for OD plasticity (31, 32), glutamatergic synapses also contribute substantially to OD plasticity (33). Both the incomplete extent of OD plasticity restoration by chondroitinase treatment and the GABA-restricted CSPG distribution led us to consider whether more widely distributed neurite-inhibiting mechanisms might participate in OD plasticity. As the vast majority of cortical neurons express NgR (Fig. 1B), we considered whether NgR-mediated myelin inhibition of neurite outgrowth contributes to closing the critical period.

Myelin-associated proteins, including ligands for NgR, are easily detected in postnatal visual cortex (Fig. 1C). The absolute abundance of the NgR ligands, Nogo-A and MAG, is essentially constant in homogenates of visual cortex over the time course of the critical period, whereas NgR tends to increase slightly (Fig. 1C). Similarly, levels of the compact myelin marker, myelin basic protein (MBP), increase only minimally during this period. A limitation of the immunoblot analysis is a mixing of all cortical layers such that selective expression changes in certain cortical layers most critical for plasticity may be obscured. Therefore, we used an immunohistochemical analysis of MBP between P26 and P60 to allow for a layer-specific assessment of expression. Although the total concentration of MBP remains

[1]Department of Neurology, [2]Department of Ophthalmology and Visual Science, Yale University School of Medicine, New Haven, CT 06520, USA.

*These authors contributed equally to this work.
†Present address: Department of Neuroscience, Albert Einstein College of Medicine, Bronx, NY 10461, USA.
‡Present address: Psychiatry and Behavioral Sciences, Baylor College of Medicine, Houston, TX 77030, USA.
§To whom correspondence should be addressed. E-mail: stephen.strittmatter@yale.edu

nearly constant, layer-specific levels of intracortical myelin mature considerably as the critical period ends (Fig. 1D). At P20 and P26, the beginning and height of the critical period, respectively, the half-maximal staining intensity is obtained at 30% of the distance from the subcortical white matter to the pial surface, whereas after the end of the critical period, at P40 and P60, this measure of myelination extends significantly further, into 50% of the cortex ($P < 0.001$) (Fig. 1E). Within layers IV and V, the relative intensity of MBP staining increases by nearly 60% and 40%, respectively. The onset and distribution of cortical myelination in mice lacking NgR is indistinguishable from that of wild-type mice (Fig. 1E). Overall, the maturation of intracortical myelination correlates with the end of the critical period.

To assess OD plasticity, we first characterized the electrophysiological responsiveness of the binocular visual cortex in NgR mutant mice exposed to unmodified visual stimuli. NgR null mice have normal vision as assayed by receptive field azimuth distribution, receptive field size, response properties, and spontaneous activity (fig. S1, A to C). The weighted ocular dominance (WOD) scores for NgR mutants and wild-type mice are comparable (Fig. 2D).

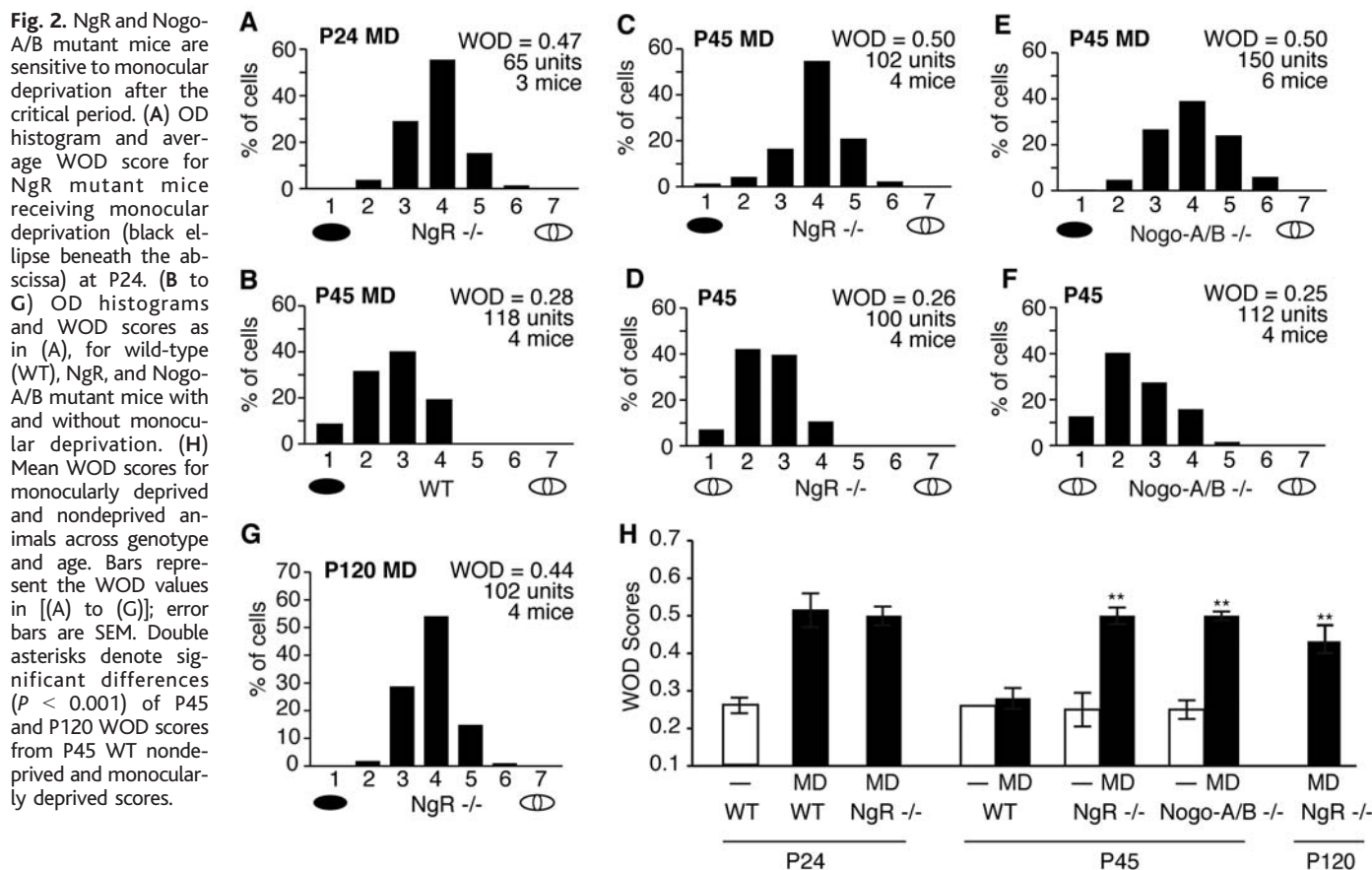To explore whether NgR regulates the magnitude of OD plasticity, we tested NgR mutant mice during the critical period. OD shifts in NgR mutant mice were induced by 4 days of monocular deprivation beginning at P24. The OD histograms and calculated WOD scores (Fig. 2A) are indistinguishable from the values for wild-type mice receiving monocular deprivation at the same age. Thus, visual system development and immature cortical plasticity are normal in the absence of NgR.

To investigate whether NgR participates in restricting OD plasticity in older animals, we deprived NgR mutants and wild-type littermates at P45, after the end of the critical period. Consistent with reported findings, 4 days of monocular deprivation do not induce an OD shift in wild-type mice (Fig. 2B). However, monocular deprivation of NgR mutant mice generates an OD shift (Fig. 2C) that differs significantly from the OD of either P45 nondeprived NgR mutant mice (Fig. 2D) or wild-type controls. Longer periods of monocular deprivation (8 days in one mouse) in NgR mutant mice beginning at P45 did not increase the magnitude of the OD shift. NgR is known to mediate myelin inhibition of neurite outgrowth; a simple model for enhanced P45 plasticity is a reduction in myelin inhibition of process growth. As the NgR ligand, Nogo-A, accounts for a considerable fraction of myelin inhibition of neurite outgrowth (9, 34, 35), a similar OD phenotype is predicted for mice lacking Nogo-A. Indeed, mice homozygous for a "gene-trap" insertion that eliminates expression of Nogo-A (and the related isoform Nogo-B) (9) display OD shifts following 4 days of monocular deprivation beginning at P45 (Fig. 2, E and F). The magnitudes of these shifts are identical to those observed with NgR mutants. Although myelinated fibers are more abundant in layers IV to VI, the OD scores from more superficial and deeper recording depths for a given penetration were indistinguishable in monocularly deprived NgR mutant mice at all ages tested.

OD plasticity at P45 in NgR and Nogo-A/B mutant mice, but not in wild-type mice, might be explained either by an absence of plasticity-limiting mechanisms or by a 2-week delay in developmental maturation of the visual cortex. Nissl staining and immunohistochemistry did not reveal any general deviation in the pace of brain development for these two strains from wild-type mice (Fig. 1). To determine whether OD plasticity persists into adulthood in NgR mutant mice, we examined mice at 4 months of age, roughly three times as old as mice at the end of the critical period. Four days of monocular deprivation is sufficient to induce OD shifts comparable to those observed in mice tested during the critical period (Fig. 2G). Therefore, a slight developmental delay in OD plasticity restriction cannot explain these findings, which indicates that NgR-dependent mechanisms participate directly in restricting visual cortex experience-dependent plasticity.

NgR signaling might function upstream in a plasticity cascade to regulate GABAergic maturation, neurotrophin levels, and/or tPA signaling. Alternatively, NgR may function downstream or

Fig. 2. NgR and Nogo-A/B mutant mice are sensitive to monocular deprivation after the critical period. (**A**) OD histogram and average WOD score for NgR mutant mice receiving monocular deprivation (black ellipse beneath the abscissa) at P24. (**B** to **G**) OD histograms and WOD scores as in (A), for wild-type (WT), NgR, and Nogo-A/B mutant mice with and without monocular deprivation. (**H**) Mean WOD scores for monocularly deprived and nondeprived animals across genotype and age. Bars represent the WOD values in [(A) to (G)]; error bars are SEM. Double asterisks denote significant differences ($P < 0.001$) of P45 and P120 WOD scores from P45 WT nondeprived and monocularly deprived scores.

independently of these mediators and limit anatomical rearrangements directly. To examine whether NgR regulates OD plasticity by modifying the GABAergic system or tPA-plasmin activity, we compared the expression of GAD65 and tPA protein in visual cortex from wild-type and NgR mutant mice (Fig. 3). Absence of NgR protein does not alter GAD65, parvalbumin, or tPA immunoreactivity in the visual cortex of P60 mice (Fig. 3, A to E), which suggests that NgR functions independently or downstream of these proteins to regulate plasticity. Dark rearing delays closure of the critical period by altering GABAergic neurotransmission (24) but does not alter the maturation of intracortical myelination, as indicated by MBP staining of sections of visual cortex in P40 mice or NgR levels (fig. S2, A and B). Thus, NgR signaling serves as a necessary gate on visual cortex plasticity. Although we cannot exclude the possibility that NgR signaling is modulated by GABA neurotransmission or tPA activity, our results support a model in which myelin and NgR function independently. These pathways presumably converge to regulate anatomical rearrangements in visual cortex.

The distribution of intracortical myelin and NgR is widespread (Fig. 1), so multiple neuronal subtypes have the potential to be regulated by this system. Given the prominence of GABAergic systems in ocular dominance plasticity, we examined the mouse visual cortex for myelinated GABAergic processes. Consistent with electron micrographs (36, 37), roughly one-third of MBP-stained visual cortex fibers are parvalbumin-positive (Fig. 3H). Because the electrophysiological recordings presented here implicate myelin-associated inhibitors as regulators of OD plasticity, it will be interesting to examine whether the NgR pathway modulates primarily GABAergic connections, dendritic spine rearrangements, or other anatomical connections.

The current study provides genetic evidence for the hypothesis that myelination consolidates neural circuitry by suppressing plasticity in the mature brain. Specifically, NgR and Nogo-A/B are required for maturation-dependent restrictions on OD plasticity to monocular deprivation in the visual cortex. However, myelin is not the only limit on cortical

plasticity, because CSPGs are also known to have a role in the visual cortex (30), and certain measures of OD persist in the adult mouse (19, 21–23). Dark rearing delays the maturation of GABAergic neurons and the deposition of CSPGs into perineuronal nets (30) but does not alter the maturation of intracortical myelination, which is controlled by developmental determinants not dependent on visual experience. Thus, at least two distinct inhibitors limit OD plasticity to the critical period, and eliminating either one is sufficient to facilitate plasticity.

The Nogo/NgR pathway is not required for closure of critical period plasticity throughout the cerebral cortex. Somatosensory barrel-field anatomical plasticity to whisker ablation is not significantly altered in Nogo-A/B mutant mice (fig. S2). Nonmyelin mechanisms may be relatively important in limiting barrel-field plasticity because the relevant critical period ends earlier in development (P1 to P4), before cortical myelination matures, or because barrel-field plasticity can be mediated subcortically (38).

Recovery of motor function after pathological damage to the mature brain is facilitated by structural and synaptic plasticity. The failure of surviving neurons to reestablish functional connectivity is most obvious after spinal cord injury, but limited axon regeneration and plasticity is central to the pathophysiology of a range of neurological disorders, including stroke, head trauma, multiple sclerosis, and neurodegenerative disease. The NgR-mediated response to myelin inhibitors is known to participate in limiting recovery from spinal cord injury and stroke (8, 10–12). Thus, brain myelin proteins impede both physiological plasticity and the repair of pathologic injury by a shared NgR mechanism.
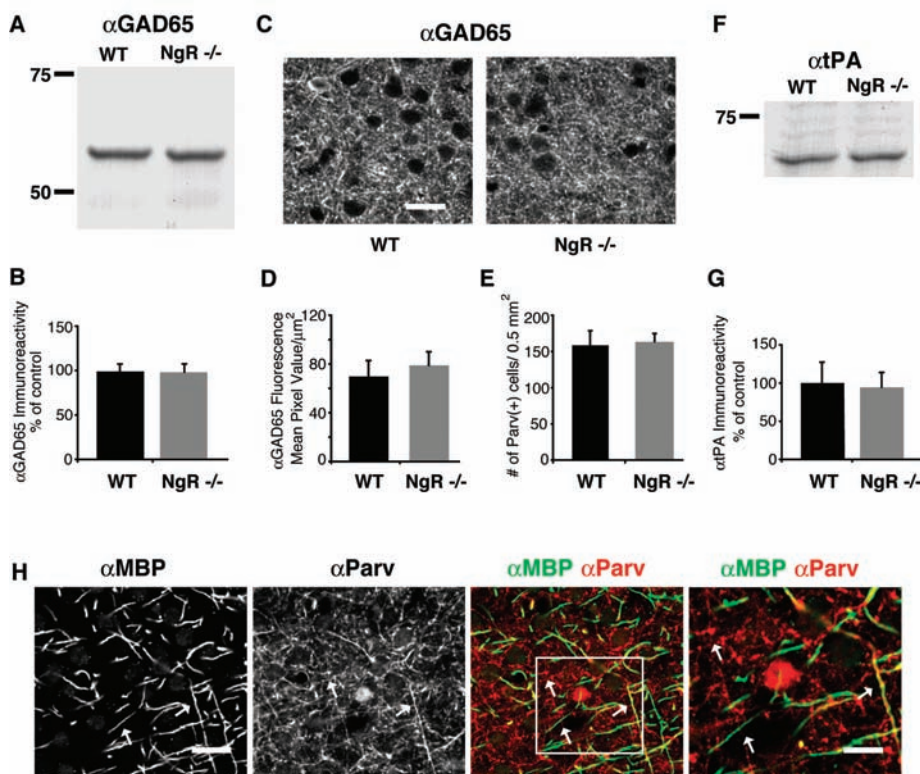

Fig. 3. GAD65 and tPA are normal in NgR mutant mice. (**A**) Homogenates of visual cortex from wild-type (WT) and NgR mice were immunoblotted with antibodies to GAD65. (**B**) Densitometry of GAD65 immunoreactivity from blots of P60 visual cortex from WT and NgR mutants ($n = 4$ mice). (**C**) P60 visual cortex of WT and NgR$^{-/-}$ mice labeled with antibodies to GAD65. (**D**) Microdensitometric level of GAD65 immunoreactivity in the neuropil of visual cortex from WT and NgR mutants. (**E**) Density of parvalbumin-immunopositive interneurons in visual cortex of WT and NgR mice, per 0.5 mm^2. (**F**) Immunoblot as in (A), with an antibody to tPA. (**G**) Quantification of tPA expression as in (B). (**H**) Confocal images of WT P60 visual cortex double-labeled with antibodies to MBP and to parvalbumin. White arrows point to immunopositive fibers in the αMBP and αParv panels, one that colocalizes in the merged image (right arrow) and others that do not (left and upper arrows). A higher magnification image, outlined by the white rectangle, is shown on the far right. Scale bar for [(C) and (H)] = 20 μm; for the higher magnification image, scale bar = 10 μm.

References and Notes

1. L. McKerracher et al., Neuron 13, 805 (1994).
2. G. Mukhopadhyay, P. Doherty, F. S. Walsh, P. R. Crocker, M. T. Filbin, Neuron 13, 757 (1994).
3. B. S. Bregman et al., Nature 378, 498 (1995).
4. M. S. Chen et al., Nature 403, 434 (2000).
5. R. Prinjha et al., Nature 403, 383 (2000).
6. T. GrandPre, F. Nakamura, T. Vartanian, S. M. Strittmatter, Nature 403, 439 (2000).
7. A. E. Fournier, T. GrandPre, S. M. Strittmatter, Nature 409, 341 (2001).
8. T. GrandPre, S. Li, S. M. Strittmatter, Nature 417, 547 (2002).
9. J. E. Kim, S. Li, T. GrandPre, D. Qiu, S. M. Strittmatter, Neuron 38, 187 (2003).
10. J. E. Kim, B. P. Liu, J. H. Park, S. M. Strittmatter, Neuron 44, 439 (2004).
11. S. Li et al., J. Neurosci. 24, 10511 (2004).
12. J. K. Lee, J. E. Kim, M. Sivula, S. M. Strittmatter, J. Neurosci. 24, 6209 (2004).
13. K. C. Wang et al., Nature 417, 941 (2002).
14. L. Schnell, M. E. Schwab, Nature 343, 269 (1990).
15. T. N. Wiesel, D. H. Hubel, J. Neurophysiol. 26, 1003 (1963).
16. D. H. Hubel, T. N. Wiesel, J. Physiol. 160, 106 (1962).
17. N. W. Daw, Visual Development (Plenum, New York, 1995).
18. J. A. Gordon, M. P. Stryker, J. Neurosci. 16, 3274 (1996).
19. N. B. Sawtell et al., Neuron 38, 977 (2003).
20. Q. S. Fischer et al., J. Neurosci. 24, 9049 (2004).
21. Y. Tagawa, P. O. Kanold, M. Majdan, C. J. Shatz, Nat. Neurosci. 8, 380 (2005).
22. T. A. Pham et al., Learn. Mem. 11, 738 (2004).
23. M. Y. Frenkel, M. F. Bear, Neuron 44, 917 (2004).

24. B. Morales, S. Y. Choi, A. Kirkwood, *J. Neurosci.* **22**, 8084 (2002).
25. G. D. Mower, *Brain Res. Dev. Brain Res.* **58**, 151 (1991).
26. T. K. Hensch *et al.*, *Science* **282**, 1504 (1998).
27. Z. J. Huang *et al.*, *Cell* **98**, 739 (1999).
28. N. Mataga, Y. Mizuguchi, T. K. Hensch, *Neuron* **44**, 1031 (2004).
29. E. J. Bradbury *et al.*, *Nature* **416**, 636 (2002).
30. T. Pizzorusso *et al.*, *Science* **298**, 1248 (2002).
31. M. Fagiolini, T. K. Hensch, *Nature* **404**, 183 (2000).
32. M. Fagiolini *et al.*, *Science* **303**, 1681 (2004).
33. S. Taha, J. L. Hanover, A. J. Silva, M. P. Stryker, *Neuron* **36**, 483 (2002).
34. M. Simonen *et al.*, *Neuron* **38**, 201 (2003).
35. B. Zheng *et al.*, *Neuron* **38**, 213 (2003).
36. J. DeFelipe, E. G. Jones, *J. Neurosci.* **5**, 3246 (1985).
37. P. Somogyi, I. Soltesz, *Neuroscience* **19**, 1051 (1986).
38. A. Rebsam, I. Seif, P. Gaspar, *J. Neurosci.* **25**, 706 (2005).
39. We thank N. Tian for providing dark-reared mice. This work was supported by grants from NIH to S.M.S. and A.W.M. and from the McKnight Founda-

Direct Evidence for a Parietal-Frontal Pathway Subserving Spatial Awareness in Humans

Michel Thiebaut de Schotten,[1] Marika Urbanski,[1] Hugues Duffau,[2] Emmanuelle Volle,[1,3] Richard Lévy,[1,4] Bruno Dubois,[1,4] Paolo Bartolomeo[1,4]*

Intraoperative electrical stimulation, which temporarily inactivates restricted regions during brain surgery, can map cognitive functions in humans with spatiotemporal resolution unmatched by other methods. Using this technique, we found that stimulation of the right inferior parietal lobule or the caudal superior temporal gyrus, but not of its rostral portion, determined rightward deviations on line bisection. However, the strongest shifts occurred with subcortical stimulation. Fiber tracking identified the stimulated site as a section of the superior occipitofrontal fasciculus, a poorly known parietal-frontal pathway. These findings suggest that parietal-frontal communication is necessary for the symmetrical processing of the visual scene.

Left unilateral neglect is a neurological condition resulting from right hemisphere damage (*1*, *2*). Neglect patients ignore left-sided events in everyday life (*3*) and have a poor functional outcome. They typically bisect horizontal lines to the right of the true center (*2*, *4*), perhaps because they perceive the left half of the line as being shorter or less salient than the right half (*5*, *6*). The study of unilateral neglect is important if we are to understand the mechanisms of spatial cognition, but its anatomical correlates are controversial. Most studies implicate the inferior parietal lobule (IPL) (*7*, *8*), consistent with the known role of posterior parietal cortex in spatial attention (*9*, *10*) and perceptual salience (*11*). Others implicate the rostral superior temporal gyrus (rSTG) (*12*), suggesting a segregation of spatial awareness in the ventral cortical visual stream (*13*, *14*). The underlying subcortical association circuits have received less attention (*15*).

We used intraoperative direct electrical stimulation (*16*) to study line bisection performance. During brain surgery for tumor resection, it is common clinical practice to awaken patients in order to assess the functional role of

[1]INSERM Unit 610, [2]Department of Neurosurgery, [3]Department of Neuroimagery, [4]Department of Neurology, Assistance Publique–Hôpitaux de Paris, Hôpital de la Salpêtrière, 75013 Paris, France.

*To whom correspondence should be addressed. E-mail: paolo.bartolomeo@chups.jussieu.fr

restricted brain regions (the brain has no receptors for pain), so that the surgeon can maximize the extent of the exeresis without provoking cognitive impairment. Patients perform cognitive tasks, such as counting or figure naming, while the surgeon temporarily inactivates restricted regions (~5 mm) around the tumor by means of electrical stimuli (*16*). If the patient stops talking or produces incorrect responses, the surgeon avoids removing the stimulated region.

CAL, a 27-year-old woman, and SB, a 28-year-old man, both left-handed, underwent surgical resection of a low-grade glioma (WHO II). In CAL, the glioma was centered on the caudal part of the right temporal lobe (*17*). CAL showed a rightward deviation upon stimulation of two cortical sites: the supramarginal gyrus (SMG, the rostral subdivision of the IPL) and the caudal portion of the superior temporal gyrus (cSTG) (Fig. 1) (table S2). There was no deviation during stimulation of the rSTG or of the frontal eye field.

In SB, the glioma was centered on the right inferior parietal lobule (*17*). SB showed a rightward deviation remarkably identical in amplitude to that shown by CAL (Fig. 2) (table S2) upon stimulation of the SMG. SB also deviated rightward during cSTG stimulation, again consistent with CAL's performance. Stimulation of other neighboring areas ("control 1" in Fig. 2B) did not determine pathological shifts. During tumor resection, subcortical regions on the floor of the surgical cavity were stimulated.

SB showed a large rightward deviation upon stimulation of the restricted region labeled as 42 in Fig. 2A, but not of neighboring cortical or subcortical areas ("control 2" in Fig. 2B). Stimulation of region 42 was repeated after additional excavation of the surgical cavity, causing even greater deviations ("O-FF 2" in Fig. 2B). Again, stimulation of neighboring subcortical sites had no effect on line bisection performance. Still further extension of the resection into the depth of the angular gyrus caused SB to deviate rightward even during stimulation of neighboring regions, or in the absence of any stimulation ("control 3" in Fig. 2B). As a consequence, the neurosurgeon decided to stop the exeresis at this level. Five days after surgery, SB accurately bisected 20-cm lines ("day +5" in Fig. 2B) and showed no signs of neglect (table S1).

Using diffusion tensor magnetic resonance tractography (*18*) on postoperative magnetic resonance imaging (MRI) scans and diffusion tensor imaging (DTI) scans, we were able to precisely map the course of long association fibers in the white matter of this patient (*19*). The region labeled as 42 in Fig. 2A, whose inactivation had produced the maximal rightward shifts on line bisection, corresponded exactly to a portion of the superior occipitofrontal fasciculus (*18*, *20*) that connects the parietal to the frontal lobe (*21*) (Fig. 2, C and D) (figs. S1 and S2). The stimulated region was both distinct and remote from other corticocortical pathways, such as the optic radiations or the parietal-temporal connections.

Our findings demonstrate that the SMG, the cSTG, and a poorly known parietal-frontal pathway, the superior occipitofrontal fasciculus (*18*, *20*), but not the rSTG, are critical to the symmetrical processing of the visual scene in humans (*22*). These results provide evidence relevant to the debate about the lesional correlates of neglect, based until now on the relatively imprecise lesion-overlapping method in stroke patients, and support the proposal that damage to the temporal-parietal junction (*7*, *8*, *23*) and the underlying white matter (*15*) is a crucial antecedent of left neglect. As a consequence, there is no need to postulate a segregation of spatial awareness, specific to humans, in the rostral part of the right STG (*14*).

We observed the maximal deviation upon inactivation of the superior occipitofrontal fasciculus in the depth of the IPL. This result specifies the precise anatomical locus of the parietal-frontal pathway in which neglect

Supporting Online Material for

Experience-Driven Plasticity of Visual Cortex Limited by Myelin and Nogo
Receptor

Aaron W. McGee, Yupeng Yang, Quentin S. Fischer,
Nigel W. Daw, Stephen M. Strittmatter*

To whom correspondence should be addressed. E-mail: stephen.strittmatter@yale.edu

This PDF file includes:

Materials and Methods
Figs. S1 to S3
References

Supplemental On-Line Material

Methods

Mouse genetic models

The Nogo-A/B gene trap and NgR gene targeted mouse strains have been described (*1, 2*). All experiments were performed on a mixed C57Bl6 and 129 mouse strain background. The targeted ES cells were derived from the 129 strain and were implanted into a C57Bl6 blastocyst. Chimeras were backcrossed to C57Bl6 mice for 4-7 generations prior to the experiments here which utilized littermate controls in all cases.

Immunohistochemistry and Immunoblotting

Mice were deeply anesthetized with intramuscular ketamine (100 mg/kg) and intraperitoneal xylazine (15 mg/kg) and perfused transcardially with PBS followed by 4% PFA in PBS. Brains were removed post-fixed for one hour. Fifty µm thick free-floating coronal sections were cut at room temperature with a vibratome. Sections were stained using standard procedures with antibodies against parvalbumin (Chemicon, 1:500), myelin basic protein (MBP) (Sternberger monoclonals, 1:500), NgR (1:500), GAD65 (R&D Systems, 10 µg/ml), Parvalbumin (Chemicon, 2 µg/ml) or with the lectin WFA (Vector labs, 5µg/ml) as indicated, followed by the appropriate Alexa488/568 secondary antibodies or for WFA, a Cy3-conjugated streptavidin (Sigma). Sections were stained with Hoescht 33342 (2µg/ml) to identify cell nuclei. Images were collected at 10X with an Olympus FV12 camera and merged with the software Photoshop (Adobe). For confocal microscopy, images were obtained from fifty-micron thick coronal sections using a 60X water immersion objective (NA 1.2) mounted on a Nikon TE2000-U

inverted microscope. Samples were scanned with a Bioradiance 2100MP laser controlled by Lasersharp acquisition software. Laser intensity, iris diameter, gain and offset settings were identical for all images collected. Images are the averages of three monoplanar scans (Kalman). Mean pixel intensity for GAD65 staining in the neuropil and the density of parvalbumin-positive neurons was performed as described by Huang et. al. (*3*) .

For immunoblotting, the binocular zone of primary visual cortex (L2-4 mm, P0-2mm) from two animals for each sample at each age was dissected away from the underlying white matter with a micro dissecting knife with the aid of a Zeiss Stemi DV4 dissecting scope under trans-illumination. The tissue was homogenized in RIPA buffer (1% Triton/0.5% sodium deoxycholate/0.1%SDS/PBS/2mm DTT). After sonication and centrifugation, supernatants were collected and protein concentrations determined with the Amersham 2D Quant kit. Multiple standards and sample duplicates were measured concomitantly to insure accuracy. 20 μg of protein was separated by SDS-PAGE and Western blotting was performed with anti-MBP, Nogo, NgR, MAG, GAD65 (0.2 μg/ml) and tPA (US Biological, 1:1000) antibodies as previously described(*2*). The specificity of the anti-tPA antibody has been demonstrated in studies of tissue from tPA -/- mouse brain (*4*).

The relative abundance of GAD65 and tPA in protein extracts from visual cortex prepared as described (above) for four samples for both genotypes Blots were developed with alkaline-phosphatase-coupled secondary antibodies (Sigma) using a chromogenic substrate. Samples were quantified as the mean density of a small rectangle enclosing the band with the 'measure' function of NIH Image version 1.63. Measurements were taken from at least three independent samples run in duplicate on the same gel for both P60 WT

and NgR KO mice. The mean density measurements for WT and NgR KO were normalized against the average for the WT samples and expressed as a percentage.

Analysis of MBP distribution

Images from anti-MBP /Alexa488 and Hoescht 33258-stained coronal sections containing visual cortex were captured at 10X and merged in Photoshop. At least two images were required to span the distance from the subcortical white matter to the pial surface. Hoescht staining was utilized to identify visual cortex prior to capturing images of MBP staining. Data points are the average of at least four sections from each of three animals for each age and genotype. Fluorescence intensity at the subcortical white matter was normalized and images were imported into NIH Image J. The relative distribution of fluorescence intensity was measured using the profile function of Image J and the corresponding pixel intensities were reported. All statistical comparisons were performed with Student's two-tailed t-test.

Electrophysiology

Electrophysiological recordings were performed under Nembutal (50 mg/kg, i.p.; Abott) /chlorprothixene (10 mg/kg, i.m; Sigma) anesthesia using standard procedures(*5*). Atropine (20mg/kg, s.c.; Optopic) was injected to reduce secretions and the parasympathetic effects of anesthetic agents, and dexamethasone (4 mg/kg, s.c.; American Reagent) was administered to reduce cerebral edema. The mouse was placed in a stereotaxic device after a tracheal tube and i.p. cannula were inserted. A craniotomy was made over the right visual cortex, and agar was applied to enhance recording

stability and prevent desiccation. The eyelids were removed from both eyes and the corneas protected thereafter by frequent application of silicon oil. Animal temperature was maintained at 37°C by a homeostatically-controlled heating pad. Heart rate and respiration were monitored continuously.

The electophysiological responses for 4-6 cells separated by > 90 μm in depth were recorded for each electrode penetration. In each mouse, 4 to 6 separate penetrations were spaced evenly at least 200 μm apart across the binocular region, defined by a RF azimuth of < 25 degrees. Cells were assigned to OD categories according to the 7-category scheme of Hubel and Wiesel[6] based on the auditory discrimination of an investigator blind to the genotype, deprivation history, and age of the animal. OD histograms were constructed and weighted ocular dominance (WOD) scores were calculated for each mouse with the formula: WOD = $(1/6G2+2/6G3+3/6G4+4/6G5+5/6G6+G7)/N$, where Gi is the number of cells in OD group i, and N is the total number of cells. Most units were also scored for noise and response strengths on a 1 (weak noise/response firing) to 3 (strong noise/response firing) scale. All comparisons were evaluated with Student's two-tailed *t*-test.
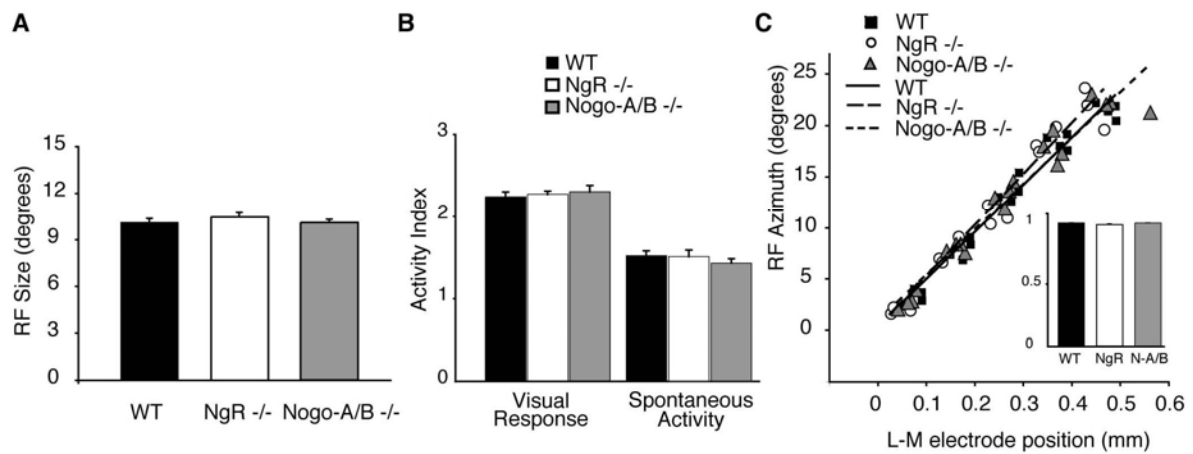
Monocular deprivation

Lid suture of the left eye was performed under 1-2% halothane anesthesia. Lid margins were trimmed and the lids sutured together using 6-0 silk. After four days of monocular deprivation the lid was opened and visual responses were recorded from animals as described[5].
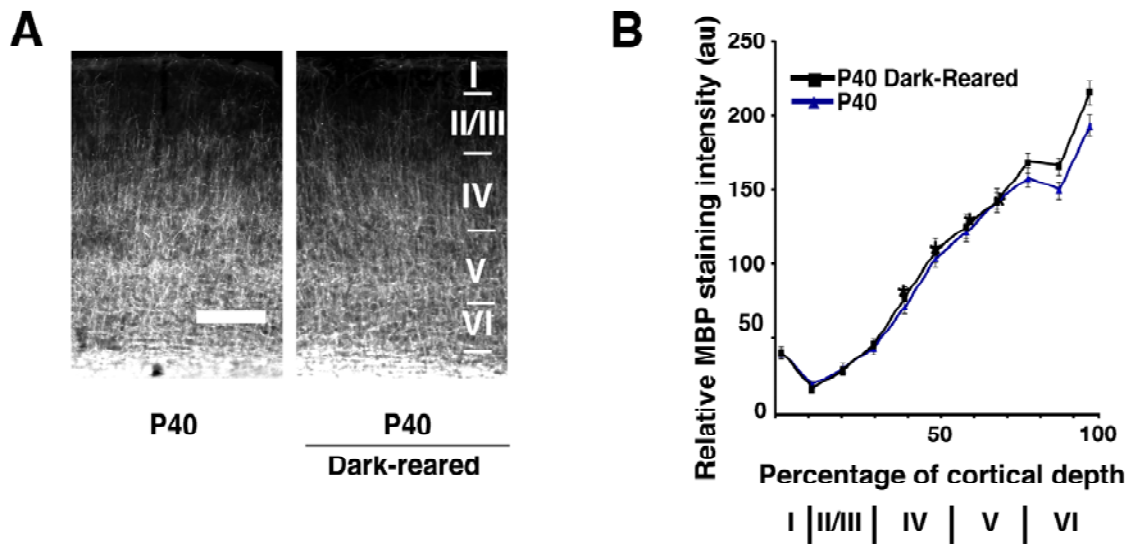
Dark rearing

Tissue from dark reared mice was generously provided by Dr. Ning Tian (Yale univ., New Haven, CT). Dark rearing methodology has been described (*7-9*).
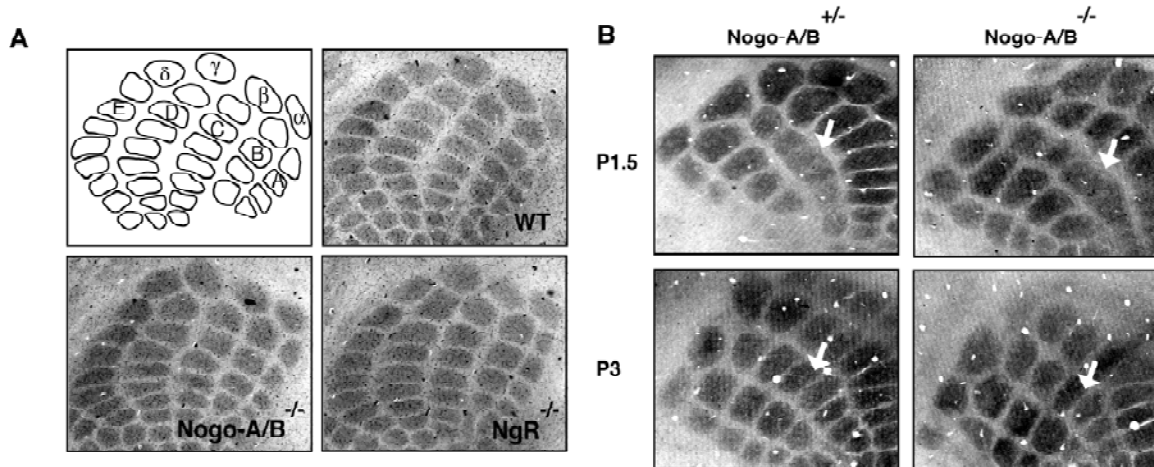
McGee et al., Suppl. Fig. 1

A

B

C

Supplemental Figure 1 Neuronal responses in visual cortex are unchanged in NgR and Nogo-A/B mutant mice. **A**, Receptive field (RF) area in wild-types (C57Bl6) (n = 8), NgR mutants (n= 8) and Nogo-A/B mutants (n = 9) (WT vs. NgR, p = 0.35; WT and N-A/B, p = 0.14). **B**, Stimulus evoked and spontaneous activity (p > 0.28 in all comparisons). **C**, Regressions of RF-center azimuth versus lateromedial electrode position for WT (black squares, n = 4), NgR (open circles, n = 3) and Nogo-A/B (grey triangles, n = 4) mutants. Insets are correlation coefficients (WT = 8, NgR = 8, Nogo-A/B = 9; WT vs. NgR, p = 0.61; WT vs. N-A/B, p = 0.14).

Supplemental Figure 2. Dark rearing does not affect the maturation of intracortical myelination in visual cortex. **A**, P40 visual cortex from normally housed (12 hr light/dark cycle) or dark-reared (24 hr dark) labelled with antibodies to MBP. Layers I-VI are indicated (right). Scale bar = 200 μm. **B**, Distribution of relative MBP intensity within visual cortex for P40 normal or dark-reared animals. Error bars = +SEM where the variance is the number of animals (n=3).

Supplemental Figure 3. Barrel plasticity is unaltered in NgR and Nogo-A/B mutant mice. A, A schematic illustrating the position of barrels corresponding to whisker rows A – E (upper left).The barrel pattern in flattened sections of somatosensory cortex revealed by cytochrome oxidase staining is indistinguishable between WT (upper right), Nogo-A/B (lower left) and NgR (lower right) mutant mice. B, Representative images of barrel cortex of Nogo-A/B mutants and heterozygous littermates following whisker ablation during (P1.5) or after (P3) the critical period. White arrows indicate the compression and fusion of barrels in the C row after whisker ablation at P1.5 but not P3.

References

1. J. E. Kim, B. P. Liu, J. H. Park, S. M. Strittmatter, *Neuron* **44**, 439 (Oct 28, 2004).
2. J. E. Kim, S. Li, T. GrandPre, D. Qiu, S. M. Strittmatter, *Neuron* **38**, 187 (Apr 24, 2003).
3. Z. J. Huang *et al.*, *Cell* **98**, 739 (Sep 17, 1999).
4. F. J. Salles, S. Strickland, *J Neurosci* **22**, 2125 (Mar 15, 2002).
5. Q. S. Fischer *et al.*, *J Neurosci* **24**, 9049 (Oct 13, 2004).
6. T. N. Wiesel, D. H. Hubel, *J Neurophysiol* **26**, 1003 (Nov, 1963).
7. N. Tian, *Vision Res* **44**, 3307 (Dec, 2004).
8. N. Tian, D. R. Copenhagen, *Neuron* **39**, 85 (Jul 3, 2003).
9. N. Tian, D. R. Copenhagen, *Neuron* **32**, 439 (Nov 8, 2001).